Classification and Composite Diagnosis of Extratropical Cyclogenesis Events in the Southwest Pacific

MARK R. SINCLAIR AND MICHAEL J. REVELL

National Institute of Water and Atmospheric Research, Ltd., Wellington, New Zealand

(Manuscript received 27 July 1998, in final form 7 May 1999)

ABSTRACT

Characteristic patterns of cyclogenesis in the southwest Pacific region are identified from a sample of 40 developing cyclones during 1990–94. Cases were chosen objectively to ensure a realistic sampling of typical rather than ''ideal'' events. A subjective classification based on synoptic-scale upper-tropospheric flow signatures prior to cyclone intensification suggested four classes into which all but three cases fell. Three categories, each containing about a quarter of the population, involved direct coupling with the upper jet. They represent cyclone formation beneath (i) the poleward exit region of a 300-hPa jet upstream from a diffluent trough (class U), (ii) the confluent equatorward entrance region of the upper wind maximum (E), and (iii) the upper jet exit region where the jet is downstream from the upper trough (class D). These are analogous to previously identified categories for the western North Atlantic region. A fourth class involved cyclones forming beneath a preexisting intense upper-level trough (class T) located poleward of the upper-level jet.

Class U cyclones, forming within diffluent airflow, exhibited strong cold fronts, weak warm fronts, and a meridional configuration while class E cyclones forming in confluent flow attained a more zonally elongated structure marked by stronger warm fronts and weak cold fronts. Class U cyclones featured frontal evolution similar to the Norwegian cyclone model while class E and D cyclones exhibited characteristics of the Shapiro–Keyser model. These results provide further observational support for the emerging paradigm of contrasting frontal and cyclone structure resulting from confluent versus diffluent large-scale flow.

1. Introduction

Over the last few decades, extratropical cyclones have been the subject of comprehensive study, often involving intensive observational campaigns. As this effort continues to uncover the rich spectrum of cyclone structures and life cycles found in nature, we have come to see cyclogenesis more as a process involving complex interactions among preexisting disturbances than as a normal mode instability problem (see Davies 1997 for a discussion). As Evans et al. (1994, hereafter E94) point out, this emerging *multibody* view of cyclogenesis implies (and explains) a huge range of possibilities by which these antecedent disturbances become properly configured for cyclogenesis to occur.

Fortunately, it appears that this diversity of development types seen in nature is amenable to categorization. This is evidenced by success in classifying cyclones on the basis of precursor synoptic-scale flow patterns (e.g., Davies et al. 1991; Thorncroft et al. 1993; Schultz et al. 1998), cloud signatures (e.g., Troup and Streten 1972; Zilman and Price 1972; Weldon 1977; Young 1993; E94), system-relative isentropic flow signatures or ''conveyor belts'' (Carlson 1980; Browning 1990), or adherence to various conceptual models (Bjerknes and Solberg 1922; Shapiro and Keyser 1990). Although satellite-based cyclone classification schemes were largely pioneered by Southern Hemisphere (SH) meteorologists (e.g., Troup and Streten 1972; Zillman and Price 1972), there has been little further attempt to advance systematic knowledge of SH cyclones, which now greatly lags that for the Northern Hemisphere (NH). The present study, which categorizes SH cyclones on the basis of precursor upper flow configurations, helps redress this imbalance.

There is much observational and theoretical evidence that there are distinct initial synoptic-scale flow patterns within the natural spectrum that lead to fundamentally different modes of cyclone evolution. Rossby and Willett (1948) suggested that during periods of strong westerlies, cyclones and their attendant frontal zones tended to elongate in the east–west direction, while higher amplitude waves associated with weaker westerlies bred cyclones possessing a more meridional structure. Sawyer (1950) further observed that cyclones with strong cold fronts were frequently found in diffluent flow such as occurs near jet exits while those within more zonal

Corresponding author address: Dr. Mark R. Sinclair, Dept. of Aeronautical Science, Embry-Riddle Aeronautical University, 3200 Willow Creek Road, Prescott, AZ 86301-3720.
E-mail: sinclam@pr.erau.edu

and confluent flow near jet entrances possessed stronger warm fronts. Modeling results (e.g., Hoskins and West 1979; Davies et al. 1991; Thorncroft et al. 1993) confirm the sensitivity of cyclone and frontal structures to the specification of the initial basic state. From the evidence of idealized simulations and observational analyses, Schultz et al. (1998) proposed that cyclones forming within a diffluent background flow become meridionally elongated with a strong cold front that rotates into a weaker warm front in the manner of the Norwegian cyclone model (e.g., Bjerknes and Solberg 1922). On the other hand, cyclones forming in confluent flow tend to acquire stronger warm fronts, a more zonally oriented structure, and to evolve according to the Shapiro–Keyser model (Shapiro and Keyser 1990), with perpendicular cold and warm fronts in a T-bone configuration and a strong bent-back occlusion. Clearly, one practical motivation for classifying cyclones is the potential to anticipate gross features of future cyclone evolution from the nature of the large-scale flow within which the incipient cyclone is embedded.

In this study, we identify characteristic patterns of cyclogenesis in the New Zealand region of the SH from a 5-yr objectively selected sample of 40 developing cyclones. These cyclones are classified on the basis of synoptic-scale upper-tropospheric flow and jet streak patterns. Composites are then constructed for each class. Our goals are to identify the characteristic precursor upper-level flow signatures conducive to cyclogenesis in this region, to determine whether these configurations lead to differing modes of cyclone evolution, and to diagnose dynamic and thermodynamic processes responsible for development of each class.

A wealth of case, composite, and modeling studies for the NH have uncovered the role of preexisting upper-level jet streaks in characteristic configurations in helping initiate and maintain surface cyclogenesis (e.g., Uccellini et al. 1984; Uccellini and Kocin 1987; Elsberry and Kirchoffer 1988). The present study is partly motivated by the success of E94 in identifying four distinctive upper-level flow and jet streak patterns accompanying surface cyclone development over the western North Atlantic. In that study, rapid cyclogenesis was found beneath the poleward exit region of a 300-hPa jet in either diffluent equatorward flow or poleward flow, beneath the equatorward entrance region, or below a double-jet structure. There is now a need to assess whether these cyclogenesis paradigms, framed almost entirely from case studies of rapid cyclogenesis conducted near North America, are applicable to other geographical regions. As the SH region considered here does not exhibit the dramatic land–sea contrasts found near North America, we might expect some differences.

Corresponding studies of the role of the upper jets for the SH are comparatively few. Sinclair and Cong (1992) showed that intensification of postfrontal cold air disturbances near Australasia coincided with the arrival of a jet streak upstream from a diffluent upper tough. On the other hand, Sinclair (1993a,b) and Pascoe et al. (1990) documented intense storms of tropical origin that were coupled with the equatorward entrance region of upper jets. These cases illustrate *possible* couplings between surface cyclones and upper jets. The present study uses a larger sample of storms to identify the possible range of cyclogenetic upper-air configurations and associated modes of cyclone evolution.

Twice-daily multilevel analyses from the European Centre for Medium-Range Weather Forecasts (ECMWF) on a $2.5° \times 2.5°$ latitude–longitude grid during 1990–94 are used for this study. While SH analyses remain hampered by a lack of data, operational numerical analysis quality over the SH has improved in recent years through use of remotely sensed data, drifting buoys, and advances in data assimilation technology (Trenberth and Olson 1988). Sinclair and Cong (1992) examined the realism of ECMWF analyses over regions between Antarctica and 50°S completely void of land-based observations. They found good correspondence between cloud and rotation features seen in satellite imagery, and the ascent and vorticity fields as analyzed by the ECMWF. We can thus have some confidence that the analyses are adequate for the present use of identifying distinctive large-scale upper flow regimes and associated cyclone and frontal orientations. However, data coverage and resolution are clearly inadequate to depict mesoscale aspects of frontal or cyclone inner-core structure. The study region (25°–50°S and 150°E–150°W) lies downwind from several rawinsonde stations near Australia and New Zealand (Fig. 1). Regions farther east void of land-based observations would still benefit from this upstream data. We have chosen to cut off our study region at 150°W, as farther east, the influence of this upstream data is probably minimal.

In this study, cyclogenesis cases are objectively chosen for the Australasian region from a global extratropical cyclone track database constructed by Sinclair (1997). Instead of limiting attention to particularly memorable storms as in E94, objective criteria based on the strength and intensification of the sea level circulation are used to make an exhaustive selection of developing cyclones during 1990–94. The 40 cyclones so found are then subjectively classified into four categories based on antecedent upper-level flow and jet streak configuration. Compositing is used to highlight persistent basic features and additional distinguishing characteristics of each class. In particular, we compare the composite frontal structure between classes to determine whether the differing kinematics of the large-scale flow at the time of cyclone formation affect the shape of the evolving surface low and the relative strengths and orientations of cold and warm fronts, as suggested by Davies et al. (1991) and Schultz et al. (1998). Finally, we examine terms in the vorticity and thermodynamic equations to diagnose forcings responsible for the development of these storms.

The next section outlines the method of selecting cas-

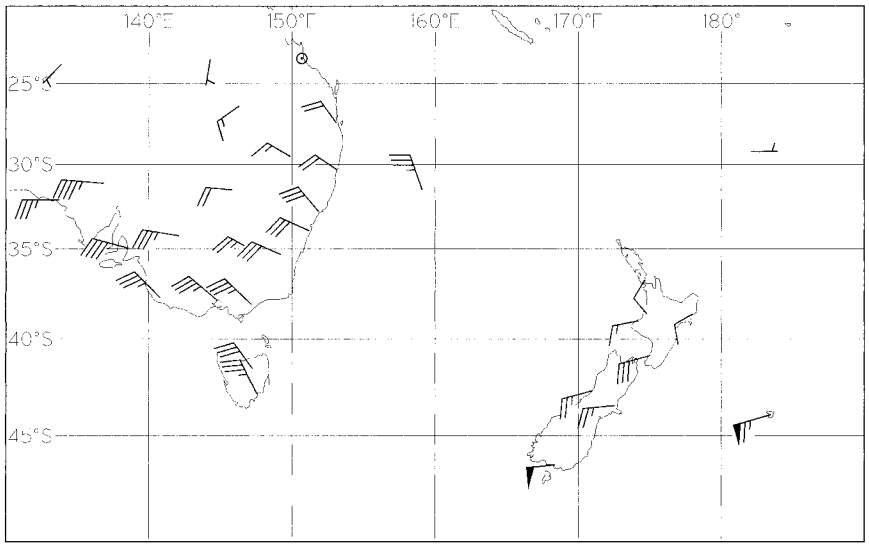

FIG. 1. Map of the eastern Australia and New Zealand regions showing locations of upper-air sounding stations.

es for study. Section 3 describes the classification and composite structure for each class while section 4 describes and presents the composite diagnostics. Results are summarized in section 5.

2. Automated case selection

In this study, cases are selected objectively to ensure that a realistic sampling of typical events is made. To avoid limiting attention to memorable or ''well behaved'' storms, developing cyclones are identified from the strength of their sea level circulation via an automated procedure. As well as avoiding subjective bias, automated procedures also streamline storm selection by avoiding laborious manual examination of large numbers of synoptic charts.

The selection procedure is based on a computer search of a database of extratropical cyclone tracks. This database is obtained via an automated cyclone finding and tracking algorithm similar to that of Sinclair (1994). Raw data composes twice-daily mean sea level (MSL) pressure analyses obtained from ECMWF on a 2.5° × 2.5° latitude–longitude grid. These analyses are first smoothed with a Cressman-type constant-radius spatial smoother to remove distortions caused by the variable grid spacing and to ensure that a fixed scale of disturbance is consistently admitted over the domain. Cyclones are then identified as local maxima of gradient wind cyclonic vorticity exceeding 1 cyclonic vorticity unit (1 CVU = -1×10^{-5} s^{-1} in the SH) and tracked using an approach based on Murray and Simmonds (1991). Detecting cyclones as vorticity rather than pressure minima makes it possible to identify incipient cyclones at an earlier stage of development, especially where a pressure minimum does not exist because of a background pressure gradient, as is common in the SH (Sinclair 1994). The cyclone center is deemed to be the point of maximum cyclonic vorticity. For each tracked cyclone, the date, position, central vorticity, pressure, and circulation are archived for each track point. Circulation, an areal measure of cyclone strength, is obtained by a method described in Sinclair (1997). The domain for each circulation calculation is the region of decreasing cyclonic vorticity surrounding the central cyclonic vorticity maximum.

The cyclone track database greatly simplifies storm selection. Cyclones occurring during 1990–94 and spending their entire life within the region bounded by 25°–50°S and 150°E–150°W are first identified by computer search of the track database. From these, a subset of developing cyclones is obtained from the track information. Central pressure fall criteria are traditionally used to identify cyclogenesis events. However, Sinclair (1995) found that central pressure change characteristics of SH cyclones are dependent on storm motion relative to the background pressure field, with cases that exhibit large pressure falls often failing to show commensurate increases in circulation. Here, we use vorticity and circulation rather than central pressure to identify developing cyclones. These kinematic quantities are also better related than pressure to socially important cyclone impacts such as strong wind and precipitation.

Following Sinclair (1995, 1997), developing cyclones are selected as those having early track points with cyclonic vorticity <4 CVU but ultimately developing a central vorticity >6 CVU and a circulation >6 circulation units (CU; 1 CU[1] = 10^7 m^2 s^{-1}). Exactly 40 such

[1] Ten CUs is roughly equivalent to a tangential wind component of 16 m s^{-1} at a radius of 1000 km.

cases were found. Imposing lower limits on both maximum track vorticity *and* circulation was found to avoid selecting small tight systems having little circulation on the one hand, or large open centers with large circulation but weak central vorticity on the other, as discussed by Sinclair (1997). The 4 CVU starting vorticity threshold eliminates cyclones that already have significant development at the first track point and so could not be properly regarded as developing. Surface plots for each event (not shown) showed that this approach consistently yielded developing cyclones of similar horizontal scale, an important requirement when compositing.

A listing of the 40 cyclogenesis events used in this study is shown in the appendix. These are organized by class (see next section). Clearly, many of these storms are weaker (in terms of central pressure falls) than the rapidly deepening cyclones classified by E94. For some of the cases here, central pressure falls are only a few hectopascals. The region of the western North Atlantic studied by E94 is one of the most cyclogenetic parts of the globe. As a result of the generally weaker storms here, we might expect characteristic jet stream signatures to be less clearly defined than in E94 and in differing configurations.

For each of the 40 cyclogenesis cases, three stages of development were identified from the track database. *Formation* was generally identified as the first track point. However, in some cases in which a weak disturbance preexisted for several days before intensifying, formation was deemed to be the time at which circulation started to increase. In such cases, a sequence of surface pressure maps was plotted to subjectively identify the most appropriate genesis time. *Development* was the time when the cyclonic circulation had the largest rate of increase (determined as a 24-h centered difference), while *maturity* was the time of maximum circulation intensity. Composites for each of these three stages were then prepared, as outlined below.

3. Classification and composite structure

a. Classification

Satellite imagery was not available for this study. Instead, we subjectively identify characteristic patterns of 300-hPa synoptic-scale flow and jet streak configuration accompanying the formation of developing South Pacific cyclones. We first plotted 300-hPa charts of geopotential and isotachs for the genesis stage of each of the 40 cases (Figs. 2–6) listed in the appendix. These plots were originally plotted on a single page (not shown) to indicate the range of upper-air flow and jet streak configurations accompanying cyclone formation. Unlike previous classification schemes, we display the entire basis set of 40 cases and not just well-behaved examples from each class. A feature common to all the cases in Figs. 2–6 is the presence of 300-hPa wind maxima exceeding 70 kt (and 100 kt in most cases). This is not surprising in view of the important role of jet streak–induced circulations in rapid cyclogenesis (Uccellini 1990). Of interest in this study is the variety of ways these jet streaks are configured relative to the incipient surface cyclone.

Our classification is subjective and is summarized in Table 1 and Figs. 2–6. Several cases have the surface cyclone forming beneath the exit region of the upper jet with the jet upstream of the upper tough (Fig. 2). Others form beneath the *entrance* region of a jet (Fig. 3). Others form beneath the exit region of a jet located downstream of the upper trough (Fig. 4), while others seem to form almost directly beneath the upper trough (Fig. 5). We now examine each in more detail.

For the 11 cases in Fig. 2, the dominant 300-hPa jet stream is located upstream from both the surface cyclone and the upper trough (see Table 1 for the requirements). This configuration of a 300 hPa jet upstream from a diffluent trough is akin to E94's comma-cloud category. The upstream wind maximum occurs in equatorward-moving or zonal flow. We call this class *upstream exit* (class U) because the dominant jet is upstream from the upper trough. Most (but not all) of the class U cases form beneath predominantly zonal upper-level flow. This is similar to the *digging trough* in which there is more cyclonic vorticity advection into the trough than out of it. For each case in this class, there was marked amplification of the upper trough, often into a closed upper low (not shown). The average maximum 24-h central pressure fall for these cases was 15 hPa (see appendix), with several events exceeding the 1 Bergeron criterion for a ''bomb'' (not shown). Sinclair and Cong (1992) found an upstream upper jet streak in equatorward-moving air (similar to the cases in Fig. 2) was necessary for development of SH cold air disturbances. In that study and the corresponding E94 class, development commences as a convective cloud cluster evolves into a baroclinic leaf, which subsequently rotates into a comma-shaped cloud system, with the entire development independent of the main polar frontal cloud band. As discussed by E94, there are analogous comma development classes in the classifications of Zillman and Price (1972), Weldon (1977), and Browning and Hill (1985). Unfortunately, satellite imagery was not available to confirm this mode of cloud evolution for the present cases.

A contrasting class, where cyclogenesis occurs beneath the confluent entrance region of a downstream wind maximum, is shown in Fig. 3.[2] Eight such class E (for *entrance*) cases were found. Some featured a second jet upstream of the upper trough, but it was more distant. The key identifying feature for class E cases is that the most dominant nearby jet streak lies *downstream*

[2] Although the jet for the 1200 UTC 29 August 1992 case (row 2) lies equatorward of the initial surface low, subsequent development (not shown) clearly occurred beneath the jet entrance.

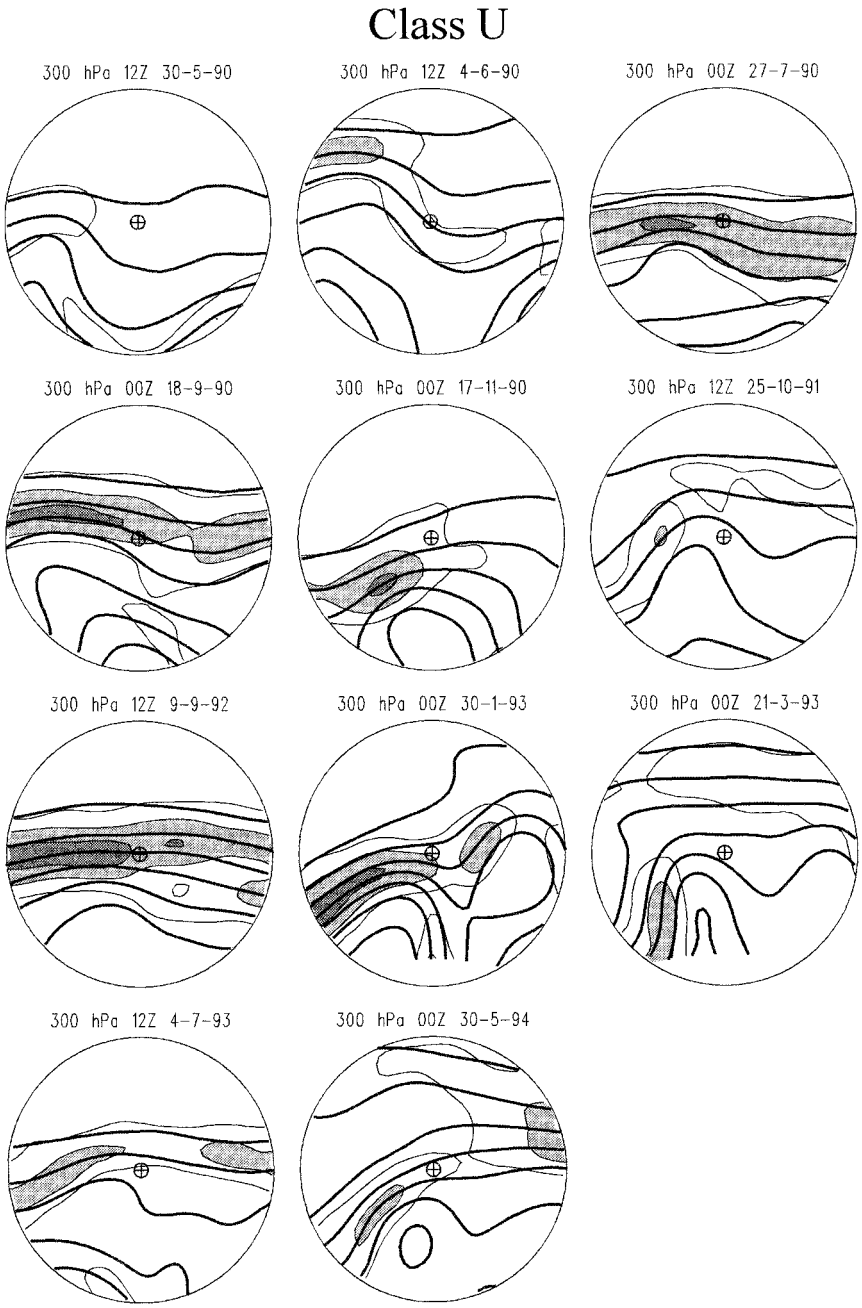

FIG. 2. The 300-hPa geopotential height (unmarked contours every 15 dam) and 70-, 100-, and 130-kt isotachs, with values >100 and 130 kt shaded, for the formation stage of the class U cases of cyclogenesis. Each circle is of radius 20° latitude (2222 km) and is centered on the 1000-hPa cyclonic vorticity maximum associated with each cyclone.

TABLE 1. Defining characteristics for the four classes.

Class	Figs.	Location of dominant upper jet	Location of incipient surface low	Character of upper flow
U (upstream exit)	2, 7	Upstream from upper trough	Beneath jet exit	Diffluent
E (equatorward entrance)	3, 8	Downstream from upper trough	Beneath jet entrance	Confluent
D (downstream exit)	4, 9	Downstream from upper trough	Beneath jet exit	Varies
T (trough)	5, 10	>800 km equatorward of upper trough	<250 km from upper trough	Sharp trough
Unclassified	6	—	—	—

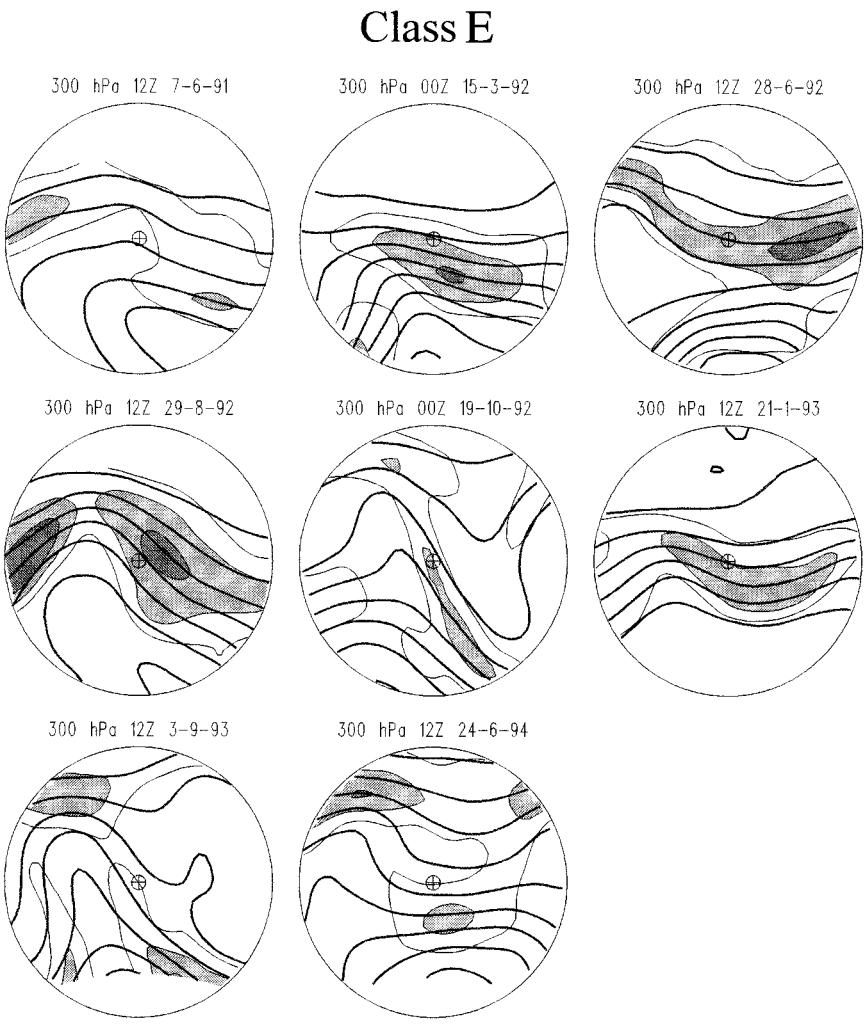

FIG. 3. As in Fig. 2 except for Class E.

from the surface low position (Table 1). Flow patterns for this class are similar to those for E94's *instant occlusion,* although their *emerging cloud head* also exhibited a downstream jet. Sinclair (1993a,b) documented two summer storms of tropical origin that were coupled with the equatorward entrance regions of anticyclonically curved upper jets. In the storm described by Sinclair (1993b), intensification coincided with the advent of a second jet into the equatorward sector. Intensification rates (see appendix) for these class E cases are similar to those for the class U cases.

A third upper-level flow signature (Fig. 4) is marked by 1000-hPa cyclogenesis occurring beneath the exit region of an upper jet, except, in contrast with class U, the jet is located downstream from the upper trough. Accordingly, we call this class *downstream exit* (class D). Eight cases are assigned to this class, which has an upper flow configuration similar to E94's *left exit* cyclogenesis. While there is sometimes a second jet downstream from the surface low, the dominant upper feature is the northwesterly jet, which is sometimes on the eastern flank of an upper trough of considerable meridional amplitude. In the corresponding left-exit category of E94, a baroclinic leaf merges with a polar front cloud band.

The fourth and final cyclogenesis category appears to not involve direct coupling with an upper jet. The eight cases in Fig. 5 feature a surface cyclone forming almost directly beneath (or within 250 km downstream from) an upper trough that already has considerable amplitude. The jet in this class is at least 800 km equatorward from the surface low. This class is called *trough* (T) because of the tendency to form almost directly beneath a preexisting upper trough. The majority of the 10 class T cases formed off the east coast of Australia. This class has no counterpart in the scheme of E94. That does not imply, of course, that similar cases do not occur in the North Atlantic. As a result of the generally weaker storms here, we might expect differing configurations from E94.

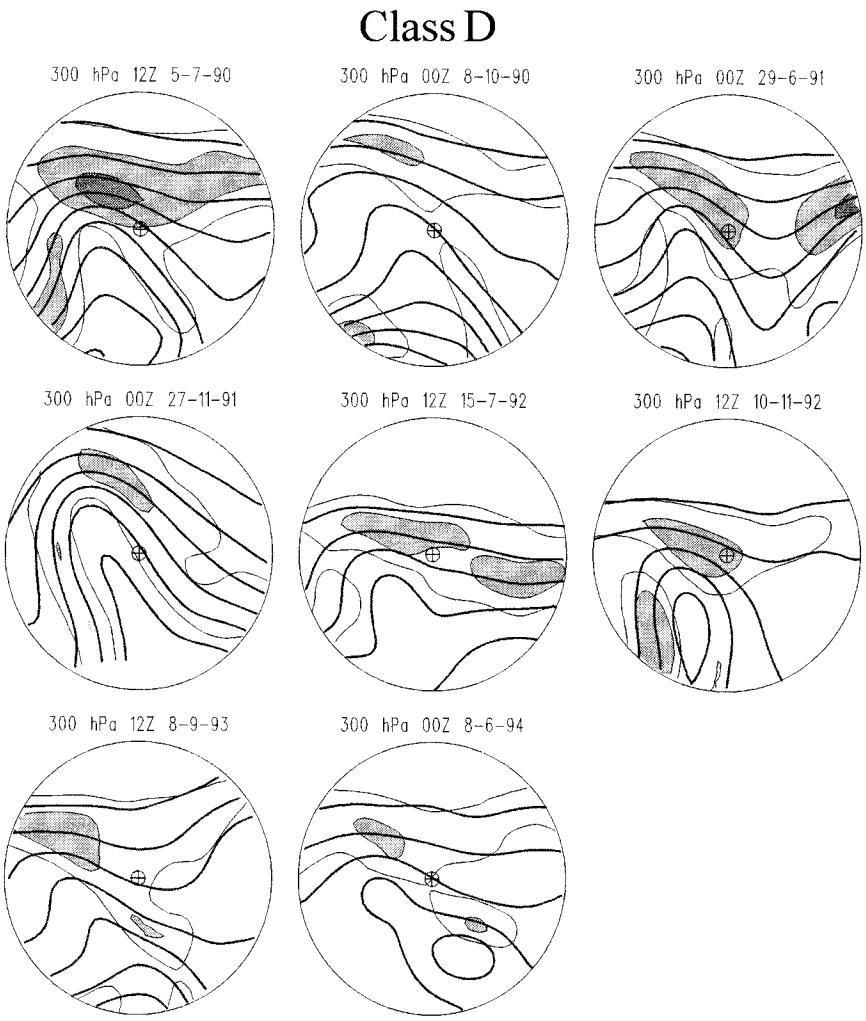

FIG. 4. As in Fig. 2 except for Class D.

Three cases were unclassified (Fig. 6). They either represented hybrids or did not fit directly into any single class. Doswell (1991) argues that any well-posed classification should contain an unclassifiable category.

This attempt to categorize SH cyclones is admittedly subjective. In a few cases distinctions between classes are small. Examples are the class D storms of 8 October 1990 and 15 July 1992 (Fig. 4), which feature a second jet to the southeast. Some class E cases feature a secondary upstream jet while some class D cases feature a second weaker jet downstream. Here, the classification is based on the location of the dominant jet at genesis. Although our goal is to identify distinctive categories, it is apparent there are one or two events where classification is less clear. Analysis uncertainty might also introduce ambiguity. As the system develops, it may also evolve into a different class. More classes might help; however, in view of the limited number of events available (40), we have restricted the number of classes to four. Three (U, E, and D) appear analogous to North Atlantic categories proposed by E94 while the fourth (T) is a new class.

Previous classification schemes typically display a single illustrative example from each class and the reader never gets to see the entire ''basis set'' of cases so as to judge the reproducibility of the classification. Here, we have chosen to display all cases involved in the classification. Furthermore, case selection here is objective and exhaustive, meaning all storms fulfilling the sea level intensity requirements have been used. In previous classifications, we are often not told how cases are selected. Commonly, well-behaved cases are chosen (nonexhaustively) from a set of memorable storms.

b. Compositing procedure

Compositing enables information from a number of examples of a phenomenon to be combined in a convenient format that highlights basic common features while eliminating detail of individual events. It has the

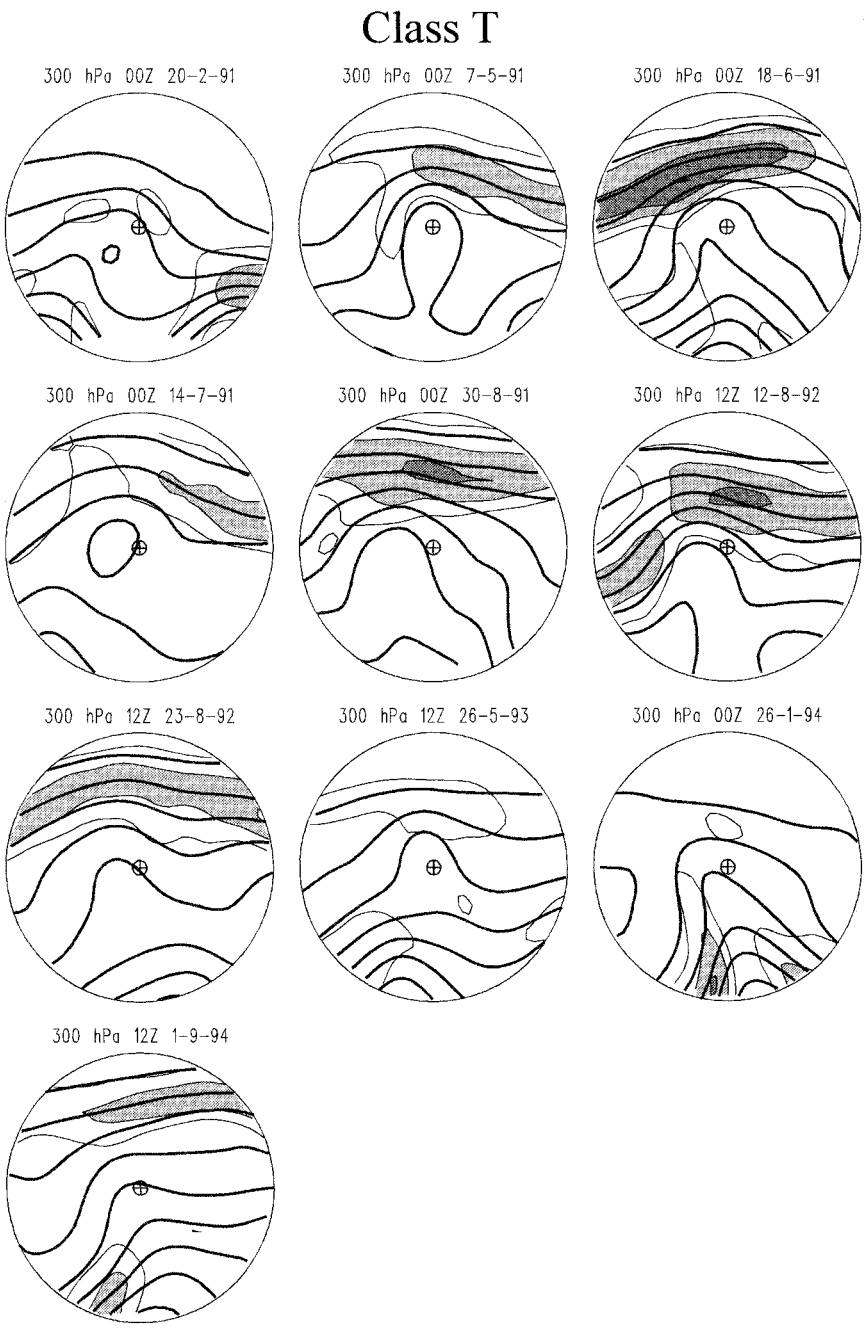

FIG. 5. As in Fig. 2 except for Class T.

potential to improve the signal-to-noise ratio of diagnostic calculations by averaging out observational and truncation uncertainty and case-to-case variability found in individual cases. The drawback of compositing is that it can blur important mesoscale detail. Thus, compositing is most useful where the events being combined are similar in as many respects as possible. Here, composites are constructed for cyclones belonging to a particular class (U, E, D, or T) at a particular stage of development (formation, development, or maturity).

Compositing is performed on a 31 × 31 Lambert conformal domain 3330 km × 3330 km in size. The compositing software centers the grid exactly on the cyclone track coordinates as read from the cyclone database for the time in question. Uninitialized analyses of H (geopotential), U and V (wind), T (temperature), relative humidity, and vertical velocity (omega) from ECMWF on a 2.5° by 2.5° latitude–longitude grid at 100, 150, 200, 250, 300, 400, 500, 700, 850, and 1000 hPa formed the basic dataset for this study. For each

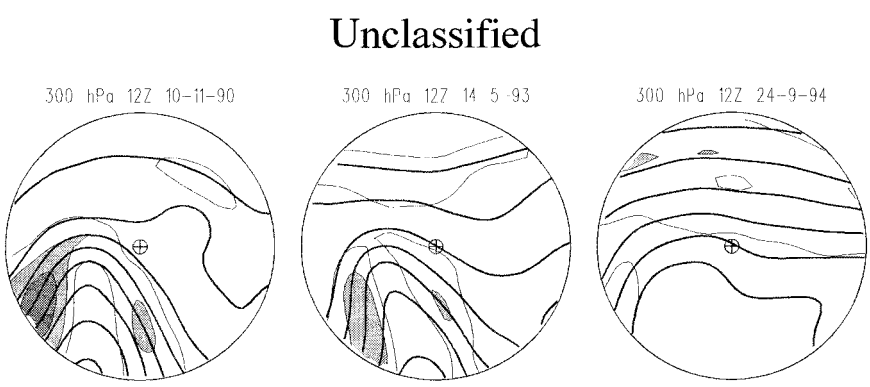

FIG. 6. As in Fig. 2 except for unclassified cases.

stage of each class, these raw fields were interpolated to the composite grid and results averaged for each grid point. Prior to averaging, each composite member was rotated to align the 500-hPa geostrophic wind vector averaged within 800 km of the grid center with the class mean. This rotation, which seldom exceeded 30°, yielded better delineation of composite upper-troposphere jet features and led to a small (average 4%) decrease in case-to-case wind speed variance (not shown). Finally, composite results are smoothed with a Cressman smoother ($r_0 = 200$ km) and displayed for formation, development, and maturity stages.

c. Upstream exit

Composites based on the 11 class U cases are shown in Fig. 7. Consistent with the class definition, the incipient surface vorticity center (marked with a C) is located beneath the poleward exit region of a jet streak located upstream from a diffluent trough embedded in predominantly zonal flow (Fig. 7a). As development progresses, the upper trough amplifies and moves closer to the surface low position while the upper jet migrates into the equatorward sector and strengthens slightly. At maturity, the surface low lies directly beneath the upper trough with the upper jet well to equatorward.

The average time interval between formation and development and between development and maturity varies from case to case. With the coarse (12 h) time resolution, these time intervals are difficult to assess reliably. On average, about 16 h elapsed between formation and development stages, and about 30 h between development and maturity. There was little variation between classes.

Along with the upper-flow patterns, we have included Ertel's potential vorticity (PV) in pressure coordinates at 300 hPa, as $-(\zeta_p + f)\partial\theta/\partial p - (\partial v/\partial p)(\partial\theta/\partial x) + (\partial u/\partial p)(\partial\theta/\partial y)$, where ζ_p is the relative vorticity on the pressure surface, and p and other symbols have their usual meanings. A significant preexisting cyclonic PV anomaly is located on the poleward flank of the approaching upper jet at genesis (Fig. 7a). Intensification of the surface low occurs beneath substantial advection of 300-hPa cyclonic PV as the PV gradient spreads over the surface low (Fig. 7b). Advection of PV in the upper troposphere can act to induce a cyclonic circulation extending throughout the troposphere to the earth's surface (Hoskins et al. 1985). Cyclogenesis occurs where and when this induced circulation reinforces the low-level circulation, which, in turn, further strengthens the upper-level PV anomaly. The strengthened PV gradient in Fig. 7b is also the result of redistribution of cyclonic PV ahead of the cyclone, possibly as the result of latent heating in the warm sector. At maturity (Fig. 7c), the westward slope with height is decreased, reducing the positive feedback between upper and lower anomalies.

In view of current interest in how the large-scale flow affects cyclone and frontal structures, we also examined the evolution of the near-surface pressure and frontal strength (Figs. 7d–f). Unfortunately, the coarse resolution of the ECMWF analyses and additional blurring associated with compositing degrade the depiction of features normally seen in mesoscale analyses of cyclones (e.g., Shapiro and Keyser 1990). Frontogenesis (shaded) is computed at 850 hPa from the composite wind and temperature fields using the Petterssen (1936) formulation for horizontal adiabatic motions, namely,

$$\frac{d}{dt}|\nabla_p\theta| = \frac{1}{2}|\nabla\theta|(E\cos 2\beta - \nabla\cdot\mathbf{V}),$$

where β is the angle between isentropes and the axis of dilatation and E is the magnitude of the total deformation, $E = (E_{st}^2 + E_{sh}^2)^{1/2}$, where $E_{st} = \partial u/\partial x - \partial v/\partial y$ and $E_{sh} = \partial v/\partial x + \partial u/\partial y$. Axes of dilatation having length proportional to E are added. Frontogenesis is strongest in regions of strong horizontal temperature gradient and flow deformation where dilatation axes are most closely aligned with isotherms. This form of the frontogenesis function neglects friction, diabatic heating, and adiabatic temperature changes associated with vertical motions.

Surface low formation (Fig. 7d) occurs within an amplifying warm tongue located within a predominantly zonal baroclinic zone. The associated frontogenesis field

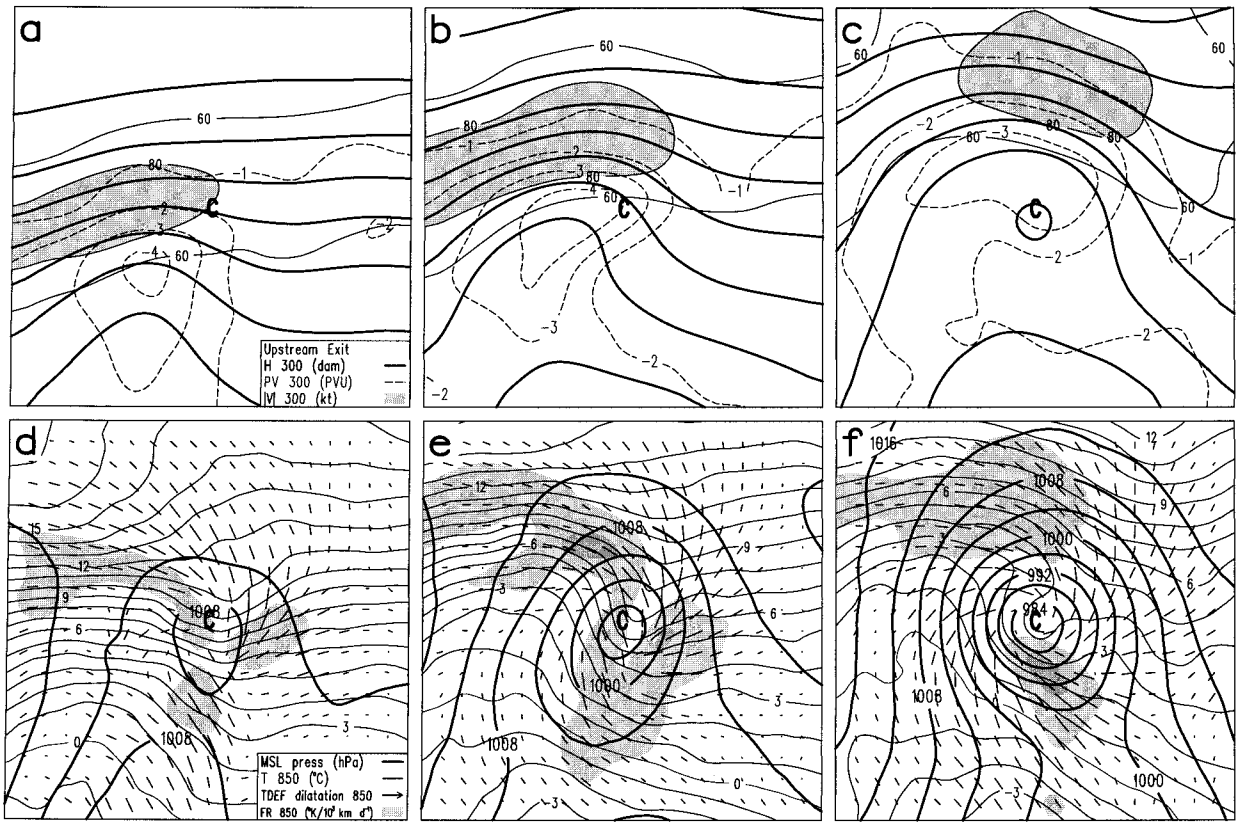

FIG. 7. Class U composites at 300 hPa (a)–(c) and near the surface (d)–(f) at three stages of development. (a)–(c) The 300-hPa geopotential (thick solid, every 10 dam, unlabeled), PV (dashed, every 1 PVU), and isotachs (thin solid, every 10 kt above 60 kt, >80 and 100 kt shaded) for (a) formation, (b) development, and (c) mature stages. (d)–(f) MSL pressure (thick solid, every 4 hPa), 850-hPa temperature (thin solid, every 1°C), orientation of the dilatation axis (line segments, length proportional to total deformation), and 850-hPa frontogenesis (>4 and 10 K per 10^3 km day^{-1} shaded) for (d) formation, (e) development, and (f) mature stages.

resembles an open wave characteristic of an incipient frontal cyclone (see Fig. 10.27 of Shapiro and Keyser 1990). As development progresses (Fig. 7e), the cold frontogenetical region west of the low migrates into the equatorward sector, catching up with the warm front east of the low, with narrowing of the warm sector reminiscent of the Norwegian cyclone model. Consistent with the diffluent flow, deformation vectors near the position of the low are preferentially oriented in the meridional direction. That part of the cold front near the low center is aligned in a north–south direction. At maturity (Fig. 7f), the composite cyclone has deepened to a central pressure of near 980 hPa, with a marked reduction in baroclinicity near the low center. The low is slightly elongated in the meridional direction. Baroclinicity and frontogenesis appear in association with the cold front in the equatorward sector, with warm sector air pinched off near the low center. A second smaller frontogenetical region resembling a bent-back front is found in the poleward sector.

These composite results concur with Schultz et al. (1998), who proposed that cyclones forming in diffluent flow possess deformation fields favoring meridional elongation of both the cyclone and the cold front, and evolve according to the Norwegian cyclone model. The present results provide observation evidence for these ideas.

d. Equatorward entrance

Class E cyclones forming beneath the equatorward entrance region of the upper-level jet (Fig. 8a) have their genesis beneath anticyclonic upper flow about 800 km downstream from the upper trough. As with the previous class U composites, development (Fig. 8b) coincides with appreciable PV advection over the surface low and with the arrival of a second jet from the west, with surface development occurring beneath the intersection of these two jets. At this stage, the composite E class has features in common with the formation stages of both class U and D events. At maturity (Fig. 8c), the downstream jet is gone and the surface low lies directly beneath the upper trough with a strengthened jet to equatorward. Although there is little change in the intensity of the PV minimum, it becomes zonally elongated along the poleward flank of the upper jet.

Surface low formation (Fig. 8d) occurs within a sharp trough of considerable meridional extent on a northwest-

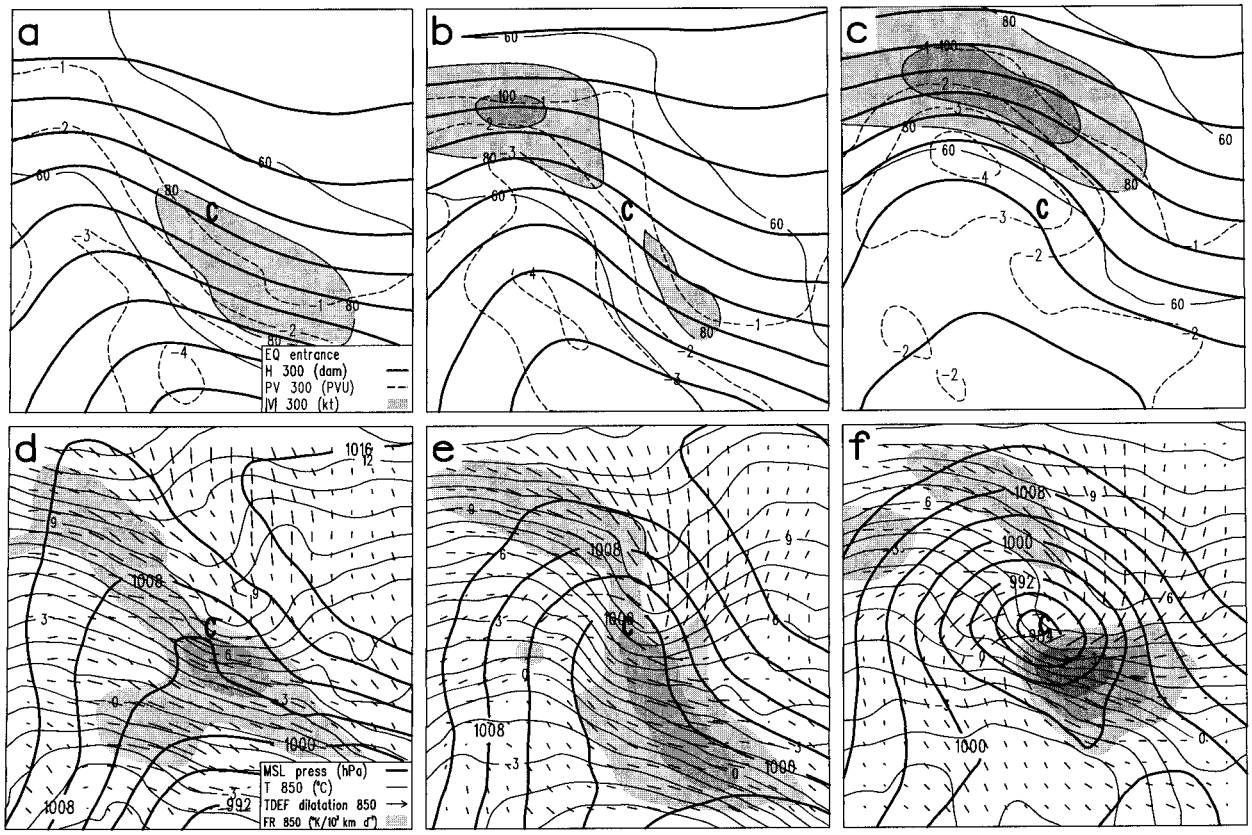

FIG. 8. As in Fig. 7 except for class E. (e) Frontogenesis exceeds 20 K per 10^3 km day^{-1} (heavy shading).

to-southeast-oriented baroclinic zone. Strongest frontogenesis (and frontal strength) is on the warm front poleward and east of the surface low, with considerable weakening near the low center as development proceeds (Figs. 8e,f). At maturity (Fig. 8f), the cyclone possesses a strong warm front and a weak cold front, aligned almost perpendicular in a manner reminiscent of a frontal T-bone configuration. Despite its meridional elongation at earlier stages of development, the mature composite storm is now elongated in the east–west direction, consistent with the predominantly zonal deformation field. These features provide some observational support for the hypotheses of Schultz et al. (1998) that cyclones in confluent flow elongate zonally and tend to acquire characteristics of the Shapiro–Keyser model.

e. Downstream exit

Class D features cyclogenesis beneath the poleward exit region of a 300-hPa jet located downstream from the upper trough (Figs. 9a,b). As with the class E composites (Fig. 8), surface development commences an average 800 km downstream from the upper trough as the upper-level PV gradient advances over the surface low position (Fig 9b), with the upper PV anomaly directly above the surface center at maturity (Fig. 9c). Of the four classes, this category features the most rapid destruction of upper-cyclonic PV and weakening of the upper jet. Low-level fields feature an intense northwest–southeast-oriented front at genesis (Fig. 9d). During development, this fractures and evolves into a classic frontal T-bone structure (Fig. 9e). The mature cyclone (Fig. 9f) has the smallest and tightest circulation of the four classes.

f. Trough

Here, although genesis occurs less than 200 km east of the upper trough, there is a marked PV gradient above the surface low position (Fig. 10a), with the composite jet at least 800 km to the north of the surface low. Intensification is associated with strengthening of this gradient (Fig. 10b), possibly in response to heating in the warm sector. Surface fields show development ahead of a preexisting thermal trough of considerable amplitude and within a cyclonically curved frontal zone bounding this cold air (Fig. 10d). Spiral arms of frontogenesis appear during development (Fig. 10e), with a strong bent-back front at maturity (Fig. 10f). Although several of these class T cases formed near the eastern coast of Australia, the surface synoptic signature in Figs.

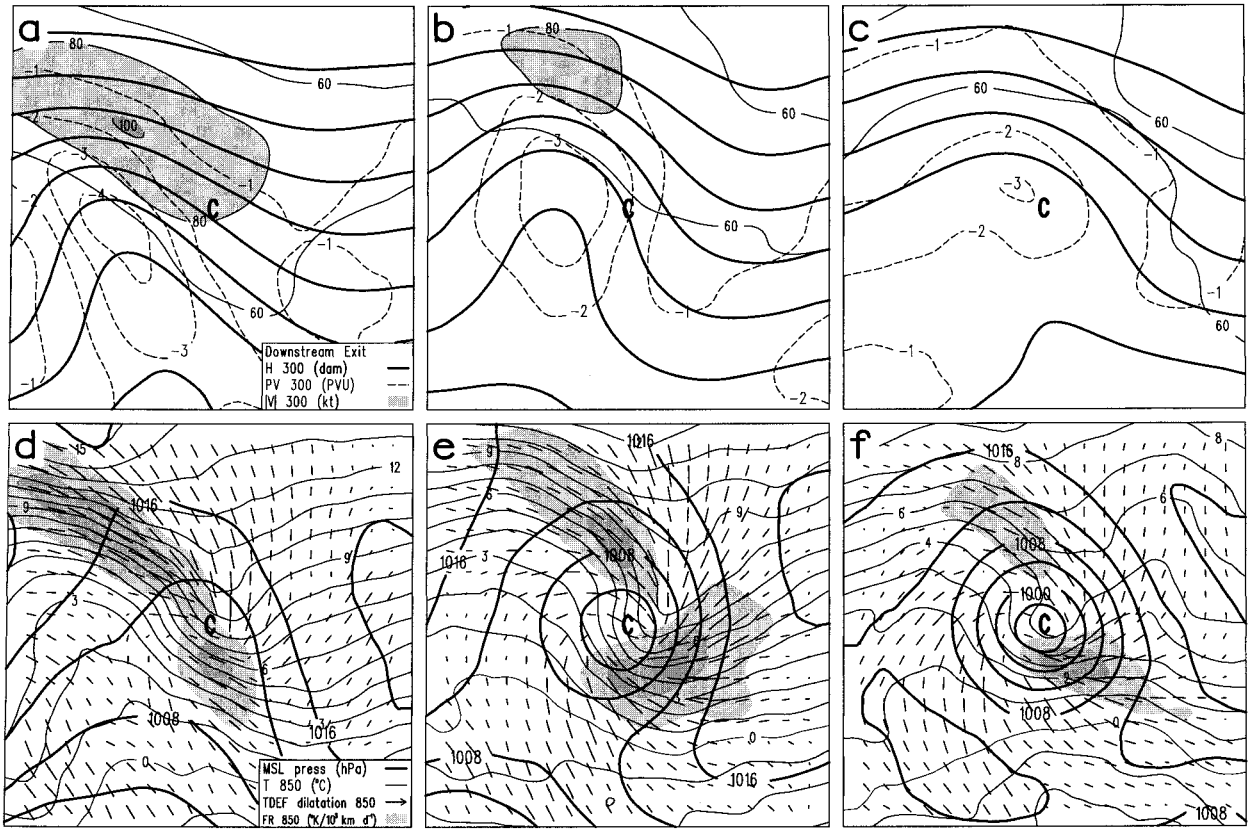

FIG. 9. As in Fig. 7 except for class D.

10d–f did not resemble the classical easterly dip[3] associated with the class of Australian east coast cyclones described by Holland et al. (1987).

4. Composite dynamics

a. Vertical profiles of vorticity and thermodynamic terms

To identify distinctive dynamical features at genesis, we looked at instantaneous terms in the vorticity and thermodynamic equations at genesis (Fig. 11). Terms in the vorticity and thermodynamic equations are reformulated in storm-following coordinates in order to separate the advective effects associated with the translation of the storm system from the processes related to storm intensification. As proposed by Johnson and Downey (1975) and applied by Sinclair and Elsberry (1986) and Sinclair and Cong (1992), the governing equation for the property of interest is expressed in the quasi-Lagrangian (QL) framework moving with velocity **C,** by replacing the Eulerian local rate of change, $\partial/\partial t$ by $\delta/\delta t - \mathbf{C}\cdot\nabla$, where $\delta/\delta t$ is the change following the storm. Here, translation velocities, **C** were obtained from the cyclone track coordinates as centered differences. The resulting QL vorticity equation in isobaric coordinates is

$$\frac{\delta\zeta}{\delta t} = -(\mathbf{V}-\mathbf{C})\cdot\nabla(\zeta+f) - (\zeta+f)\nabla\cdot\mathbf{V} - \omega\frac{\partial\zeta}{\partial p} + \left(\frac{\partial u}{\partial up}\frac{\partial\omega}{\partial y} - \frac{\partial v}{\partial p}\frac{\partial\omega}{\partial x}\right), \quad (1)$$

where ζ is the relative vorticity, ω is the vertical velocity, and other symbols have their usual meanings. At the coarse resolution used here, vertical advection and twisting [last two terms of (1)] were found to be negligible compared with the other terms and so are not shown.

Similarly, the thermodynamic equation in QL coordinates is

$$\frac{\delta T}{\delta t} = -(\mathbf{V}-\mathbf{C})\cdot\nabla T + S\omega + \frac{\dot{Q}}{c_p}, \quad (2)$$

where $S = -T\partial\ln\theta/\partial p$ is a static stability parameter and $\dot{Q}/c_p$ is the diabatic heating rate. Diabatic heating, assumed to arise entirely from release of latent heat of condensation during saturated adiabatic ascent, was approximated following Haltiner and Williams (1980, p. 309).

[3] An *easterly dip* is a trough that forms on the equatorward side of an anticyclone near the east coast of Australia. It is occasionally a precursor to more vigorous cyclogenesis.

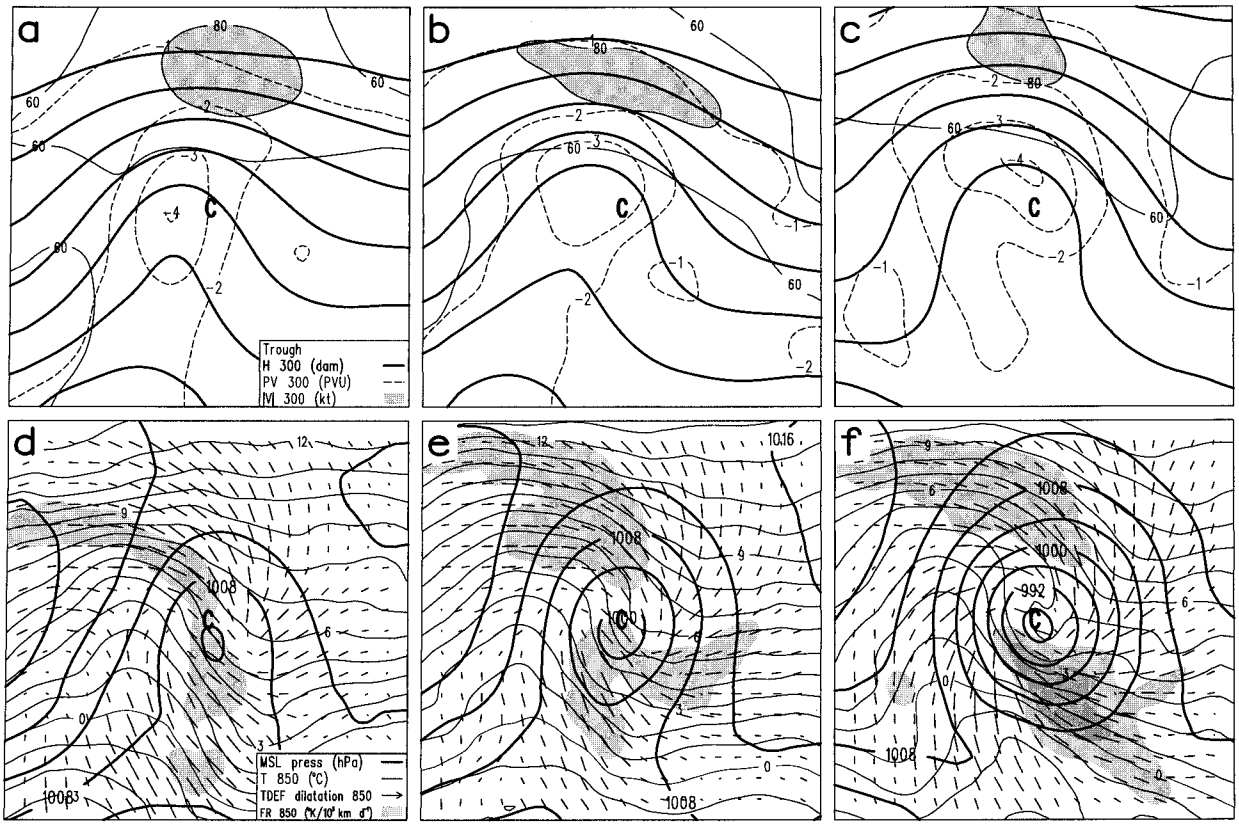

FIG. 10. As in Fig. 7 except for class T.

Vorticity terms (Figs. 11a–d) exhibit general features of upper-level QL cyclonic vorticity advection (CVA) (solid) offset by divergence (dashed), with vorticity generation by convergence at lower levels for all four classes. In the absence of twisting and vertical advection, the sum of these terms, which equates to $-\nabla \cdot [(\mathbf{V} - \mathbf{C})(\zeta + f)]$, should correspond to the instantaneous vorticity tendency following the storm. This term (dotted)

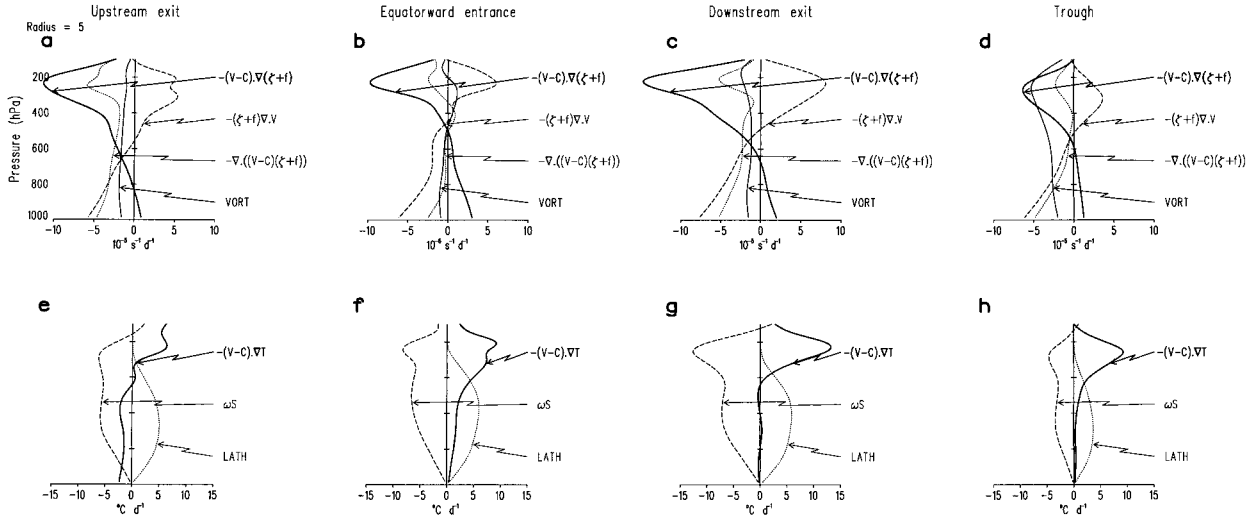

FIG. 11. Formation stage composite vertical profiles for the four classes of indicated (a)–(d) vorticity and (e)–(h) thermodynamic equation terms, averaged over the 5° lat (555 km) radius circle centered on each cyclone. Vorticity equation terms are in units of 10^{-5} s^{-1} day^{-1}, thermodynamic in °C day^{-1}. All terms are spatially averaged over the 555-km radius circle centered on each 1000-hPa cyclonic vorticity maximum.

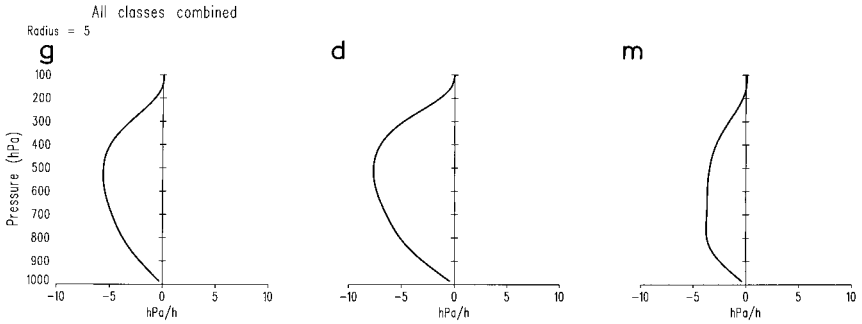

FIG. 12. Composite p vertical velocity profiles (hPa h^{-1}) averaged over the 555-km radius circle centered on each cyclone for each of the three stages of development: (g) genesis, (d) development, and (m) maturity.

is cyclonic throughout the troposphere, particularly near the surface and tropopause, levels where it is most likely offset by friction. The profile of relative vorticity (thin solid) for the class E storms (Fig. 11b) shows cyclonic vorticity at lower levels with anticyclonic flow aloft. In contrast, the class T cyclones exhibit a cold-core structure of strong cyclonic vorticity aloft with weaker cyclonic vorticity near the surface (Fig. 11d).

Thermodynamic terms (Figs. 11e–h) show latent heating from saturated adiabatic ascent, offset by adiabatic cooling, ωS, for all four classes. These terms will exactly offset each other for saturated ascent along a moist adiabat. The adiabatic cooling increases above 250 hPa because of the sudden jump in S above the tropopause. This cooling aloft is offset by warm advection, a feature noted in other diagnoses of developing cyclones (e.g., Rausch and Smith 1996). Isobaric warm air advection at these levels can be indicative of tropopause folding that results in warmer stratospheric air west of the surface low and a high, cold tropopause to the east (Hirschberg and Fritsch 1991).

These results show that cyclogenesis occurs in the presence of CVA and divergence aloft, with latent heat release offset by adiabatic cooling being the dominant thermodynamic terms. It is difficult to conceive of extratropical cyclogenesis without these features. To identify which forcings modulate surface development, 24-h surface pressure falls were correlated (not shown) with the various terms in (1) and (2) averaged over the same 24-h period. For all classes and stages of development, mid- and upper-level advection of vorticity by the storm-relative flow was consistently the term most highly correlated with cyclone deepening, with correlations in the range 0.65 to 0.95. Sanders (1986), among others, also found that midtropospheric vorticity advection was highly correlated with cyclone deepening. For class E, these correlations exceeded 0.9, suggesting that net influx of cyclonic vorticity aloft is especially significant in modulating surface development for this class. This is consistent with Fig. 8b, which suggests that cyclogenesis for this class is triggered by the arrival of a second jet in the equatorward sector.

When the usual Eulerian form of vorticity advection, $-\mathbf{V}\cdot\nabla\zeta$, is used, the correlation with storm deepening rates falls to less than 0.5. This underscores the fact that it is advection by the storm-relative flow, $-(\mathbf{V}-\mathbf{C})\cdot\nabla(\zeta+f)$, that modulates cyclogenesis. The subtracted component, $-\mathbf{C}\cdot\nabla(\zeta+f)$, simply moves the vorticity pattern around without development. Because $\mathbf{V}-\mathbf{C}$ is also a measure of the basic flow baroclinicity, development will only occur where CVA is found within a baroclinic current. The greatest loss of column mass by divergence aloft will tend to focus on regions of strongest storm-relative CVA, which maximizes in the vicinity of the upper jet where $|\mathbf{V}| \gg |\mathbf{C}|$ and where vorticity gradients are large. This corroborates the general view that cyclogenesis is typically found in close association with jet streaks and justifies our search for characteristic upper-level jet streak patterns.

b. Vertical velocity

Finally, we briefly examined vertical motion for each stage of all the classes. The ECMWF omega fields were spatially averaged within the 555-km circle centered on each 1000-hPa vorticity maximum and results composited. Resulting vertical motion profiles differed little between classes, perhaps as a result of the spatial averaging. Greatest changes are seen during the life of the storms. Combined results for the three stages (Fig. 12) reveal strongest ascent at the development stage, with the level of maximum ascent lowering during the life of the cyclone. Calculations (not shown) of the various components of the quasigeostrophic vertical velocity, based on the partitioning proposed in the appendix of Hoskins et al. (1985), suggest this lowering is due to increasing frictional convergence and the tendency for Ekman pumping to dominate as the cyclone matures. These calculations also showed that adiabatic terms accounted for most of the vertical motion at this resolution, a surprising result considering the primary

role of latent heating in forcing vertical motion for Australian east coast cyclones (Revell and Ridley 1995). Initial mesoscale model calculations at 40-km resolution for one of the present storms yielded a greater role for diabatic heating, suggesting that the discrepancy is probably a resolution problem.

5. Summary and conclusions

This study classifies extratropical cyclogenesis in the southwest Pacific on the basis of synoptic-scale upper-tropospheric flow and jet streak signatures prior to cyclone intensification. Developing cyclones were selected from a cyclone track database. Case selection was objective to reduce subjective bias and to ensure that typical rather then ideal cases were chosen. A total of 40 developing cyclones occurring between 1990 and 1994 were selected for the midlatitude region of the southwest Pacific centered on New Zealand. From these, we subjectively identified four classes and constructed composites from ECMWF analyses for formation, development, and mature stages of each class.

Three categories, each containing about a quarter of the population, involved direct coupling with the upper jet. Development for these cases occurred as a region of appreciable advection of cyclonic PV spread over the surface low. One class involving cyclone formation beneath the poleward exit region of a 300-hPa jet upstream from a diffluent trough (class U) intensifies as the upper jet propagates through the equatorward sector. Consistent with the jet pattern, composites for this class exhibited a relatively strong (weak) cold (warm) front during development and evolve in a manner reminiscent of the Norwegian cyclone model. A contrasting class, where the surface cyclone forms beneath the confluent equatorward entrance region of a downstream jet streak (class E), exhibits a markedly stronger warm front and a more zonally oriented mature structure. Intensification coincides with arrival of a second jet equatorward of the cyclone center, with the mature stage exhibiting the mutually perpendicular cold and warm fronts seen in the Keyser–Shapiro model. These contrasting composite results provide more general observational support for the contrasting realizations of cyclone and frontal structure for confluent versus diffluent flow, first noted by Rossby and Willett (1948) and Sawyer (1950), and analyzed in more detail by Schultz et al. (1998). Composites for the third class, involving cyclogenesis beneath the upper jet exit region of a jet located downstream from the upper trough (class D), also exhibited perpendicularly oriented cold and warm fronts.

These three classes have flow features in common with the western North Atlantic classification of E94, suggesting a wider applicability of these precyclogenetic modal patterns. A fourth class involves cyclogenesis beneath an intense preexisting upper-level trough (class T) located at least 800 km poleward of the upper jet. Despite an apparent near-vertical structure at genesis, there was still sufficient westward tilt with height to yield a gradient of PV above the surface low. This upper-level gradient strengthened in response to PV destruction downstream, possibly in response to warm sector heating over the warm East Australia Current.

Vorticity and thermodynamic equation diagnostics revealed that the terms forcing cyclogenesis were CVA and divergence aloft, coupled with latent heat release offset by adiabatic cooling, as in other studies. Advection of vorticity by the storm-relative flow aloft was the factor best correlated with surface development. Correlations exceeded 0.9 for class E storms for which cyclogenesis is triggered by a second jet propagating into the equatorward sector. The dominant role of storm-relative CVA identified by this study underscores the fact that cyclogenesis tends to occur beneath regions of CVA where $|\mathbf{V}| \gg |\mathbf{C}|$, implying vertical shear and strongest vorticity gradients. Such regions are principally found in close association with jet streaks, justifying our search for characteristic upper-level jet streak patterns.

Future work includes constructing a more rigorous and repeatable classification using objective cluster or principal component analysis of upper-air patterns, based on a much larger sample of developing cyclones. Use of fully automated cyclone selection and classification procedures will enable principal modes of cyclogenesis to be readily identified for any part of the world. Of interest is how these modes might be related to the planetary-scale flow and to indices of low-frequency variability like ENSO and zonal wind vacillation. The present synoptic classification based on manual examination of individual cases will aid in interpreting results from such a fully automated classification scheme.

Acknowledgments. Gridded atmospheric analyses were provided by the ECMWF. This work was supported by the New Zealand Foundation for Research, Science and Technology. We are grateful to Dr. David Schultz for helpful comments on an earlier draft of this manuscript. The comments of three reviewers also led to improvements in the manuscript.

APPENDIX

Cyclogenesis Events Used in this Study

Listing by category of the 40 cyclogenesis events used in this study. The dates span formation through maturity stages (see section 2 for definition) while the locations refer to the position where maximum intensification occurs. The minimum central pressure, largest 24-h central pressure fall, and overall circulation increase over the life of each storm are also shown.

TABLE A1. Cyclogenesis events used in this study.

Class (N)	Period	Development location	Min pressure (hPa)	Max 24 h fall (hPa)	Circulation increase (CU)
U (11)	30 May–2 Jun 1990	37°S, 155°E	984	16	7.7
	4–6 Jun 1990	40°S, 174°W	984	16	5.8
	27–29 Jul 1990	32°S, 158°E	986	18	6.3
	17–19 Sep 1990	36°S, 152°W	986	19	9.5
	17–19 Nov 1990	36°S, 168°E	990	13	6.4
	25–27 Oct 1991	37°S, 159°E	998	9	3.8
	9–12 Sep 1992	37°S, 168°W	981	12	4.6
	30–31 Jan 1993	45°S, 178°W	973	23	7.4
	21–22 Mar 1993	41°S, 179°W	986	11	2.5
	4–8 Jul 1993	32°S, 171°W	994	11	5.0
	30 May–1 Jun 1994	41°S, 170°W	977	17	10.5
Avg.			985	15	6.3
E (8)	7–9 Jun 1991	29°S, 174°W	982	15	7.0
	15–16 Mar 1992	40°S, 160°E	973	30	8.7
	28–30 Jun 1992	34°S, 171°W	974	23	8.4
	29–31 Aug 1992	37°S, 169°W	980	13	6.5
	19–21 Oct 1992	35°S, 165°E	1003	4	4.7
	21–23 Jan 1993	44°S, 178°E	974	20	6.0
	3–5 Sep 1993	39°S, 173°E	1001	2	6.8
	24–27 Jun 1994	43°S, 172°W	979	8	4.1
Avg.			983	14	6.5
D (8)	5–8 Jul 1990	39°S, 160°E	994	9	2.6
	8–10 Oct 1990	35°S, 165°W	1004	8	5.0
	28–30 Jun 1991	40°S, 150°E	997	14	7.0
	27–29 Nov 1991	45°S, 159°W	978	16	5.6
	15–17 Jul 1992	32°S, 169°W	1004	7	2.6
	10–13 Nov 1992	36°S, 160°E	1001	6	5.2
	8–10 Oct 1993	39°S, 157°E	1005	6	4.2
	8–10 Jun 1994	38°S, 161°E	996	8	6.7
Avg.			997	9	4.9
T (10)	20–22 Feb 1991	44°S, 172°W	994	6	3.8
	7–9 May 1991	35°S, 172°W	997	7	4.1
	17–21 Jun 1991	37°S, 168°W	972	11	9.2
	14–16 Jul 1991	35°S, 156°E	998	8	2.7
	30–31 Aug 1991	43°S, 153°E	997	3	2.7
	12–13 Aug 1992	38°S, 160°E	980	15	3.0
	23–26 Aug 1992	34°S, 164°E	977	22	11.0
	26–28 May 1993	33°S, 176°E	984	14	6.6
	26–28 Jan 1994	38°S, 171°W	989	12	8.0
	1–3 Oct 1994	34°S, 175°E	1007	1	2.0
Avg.			990	10	5.3
Unclassified (3)	10–13 Nov 1990	40°S, 160°E	997	5	2.5
	14–16 May 1993	39°S, 168°E	998	9	5.9
	24–27 Oct 1994	41°S, 178°W	984	11	3.5

REFERENCES

Bjerknes, J., and H. Solberg, 1922: Life cycle of cyclones and the polar front theory of atmospheric circulation. *Geofys. Publ.,* **3** (1), 1–18.

Browning, K. A., 1990: Organization of clouds and precipitation in extratropical cyclones. *Extratropical Cyclones. The Erik Palmén Memorial Volume,* C. W. Newton and E. O. Holopainen, Eds., Amer. Meter. Soc., 129–153.

——, and F. F. Hill, 1985: Mesoscale analysis of a polar trough interacting with a polar front. *Quart. J. Roy. Meteor. Soc.*, **111,** 445–462.

Carlson, T. N., 1980: Airflow through midlatitude cyclones and the comma cloud pattern. *Mon. Wea. Rev.*, **108,** 1498–1509.

Davies, H. C., 1997: Emergence of the mainstream cyclogenesis theories. *Meteor. Z.*, **6,** 261–274.

——, C. Schär, and H. Wernli, 1991: The palette of fronts and cyclones within a baroclinic wave development. *J. Atmos. Sci.,* **48,** 1666–1688.

Doswell, C. A., 1991: Comments on ''Mesoscale convective patterns of the southern high plains.'' *Bull. Amer. Meteor. Soc.*, **72,** 389–390.

Elsberry, R. L., and P. J. Kirchoffer, 1988: Upper-level forcing of explosive cyclogenesis over the ocean based on operationally analyzed fields. *Wea. Forecasting,* **3,** 205–216.

Evans, M. S., D. Keyser, L. F. Bosart, and G. M. Lackmann, 1994: A satellite-derived classification scheme for rapid maritime cyclogenesis. *Mon. Wea. Rev.*, **122,** 1381–1416.

Haltiner, G. J., and R. T. Williams, 1980: *Numerical Prediction and Dynamic Meteorology.* John Wiley and Sons, 477 pp.

Hirschberg, P. A., and J. M. Fritsch, 1991: Tropopause undulations and the development of extratropical cyclones. Part I: Overview and observations from a cyclone event. *Mon. Wea. Rev.,* **119,** 496–517.

Holland, G. J., A. J. Lynch, and L. M. Leslie, 1987: Australian east-coast cyclones. Part I: Synoptic overview and case study. *Mon. Wea. Rev.,* **115,** 3024–3036.

Hoskins, B. J., and N. V. West, 1979: Baroclinic waves and frontogenesis. Part II: Uniform potential vorticity jet flows—Cold and warm fronts. *J. Atmos. Sci.,* **36,** 1663–1680.

——, M. E. McIntyre, and A. W. Robertson, 1985: On the use and significance of isentropic potential vorticity maps. *Quart. J. Roy. Meteor. Soc.,* **111,** 877–946.

Johnson, D. R., and W. K. Downey, 1975: Azimuthally averaged transport and budget equations for storms: Quasi-Lagrangian diagnostics 1. *Mon. Wea. Rev.,* **103,** 967–979.

Murray, R. J., and I. Simmonds, 1991: A numerical scheme for tracking cyclone centres from digital data. Part I: Development and operation of the scheme. *Aust. Meteor. Mag.,* **39,** 155–166.

Pascoe, R. M., J. H. A. Lopdell, and M. R. Sinclair, 1990: The Canterbury/Kaikoura storm of January 19, 1988. *Wea. Climate,* **10,** 16–23.

Petterssen, S., 1936: Contribution to the theory of frontogenesis. *Geofys. Publ.,* **11** (6), 1–27.

Rausch, R. L. M., and P. J. Smith, 1996: A diagnosis of a model-simulated explosively developing extratropical cyclone. *Mon. Wea. Rev.,* **124,** 875–904.

Revell, M. J., and R. R. Ridley, 1995: The origin and evolution of low-level potential vorticity anomalies during a case of Tasman Sea cyclogenesis. *Tellus,* **47A,** 779–796.

Rossby, C.-G., and H. C. Willett, 1948: The circulation of the upper troposphere and lower stratosphere. *Science,* **108,** 643–652.

Sanders, F., 1986: Explosive cyclogenesis in the west-central North Atlantic Ocean, 1981–1984. Part I: Composite structure and mean behavior. *Mon. Wea. Rev.,* **114,** 1781–1794.

Sawyer, J. S., 1950: Formation of secondary depressions in relation to the thickness pattern. *Meteor. Mag.,* **79,** 1–5.

Schultz, D. M., D. Keyser, and L. F. Bosart, 1998: The effect of large-scale flow on low-level frontal structure and evolution in mid-latitude cyclones. *Mon. Wea Rev.,* **126,** 1767–1791.

Shapiro, M. A., and D. Keyser, 1990: Fronts, jet streams, and the tropopause. *Extratropical Cyclones. The Erik Palmén Memorial Volume,* C. W. Newton and E. O. Holopainen, Eds., Amer. Meteor. Soc., 167–191.

Sinclair, M. R., 1993a: Synoptic-scale diagnosis of the extratropical transition of a southwest Pacific tropical cyclone. *Mon. Wea. Rev.,* **121,** 941–960.

——, 1993b: A diagnostic study of the extratropical precipitation resulting from Tropical Cyclone Bola. *Mon. Wea. Rev.,* **121,** 2690–2707.

——, 1994: An objective cyclone climatology for the Southern Hemisphere. *Mon. Wea. Rev.,* **122,** 2239–2256.

——, 1995: A climatology of cyclogenesis for the Southern Hemisphere. *Mon. Wea. Rev.,* **123,** 1601–1619.

——, 1997: Objective identification of cyclones and their circulation intensity, and climatology. *Wea. Forecasting,* **12,** 595–612.

——, and R. L. Elsberry, 1986: A diagnostic study of baroclinic disturbances in polar air streams. *Mon. Wea. Rev.,* **114,** 1957–1983.

——, and X. Cong, 1992: Polar air stream cyclogenesis in the Australasian region: A composite study using ECMWF analyses. *Mon. Wea. Rev.,* **120,** 1950–1972.

Thorncroft, C. D., B. J. Hoskins, and M. E. McIntyre, 1993: Two paradigms of baroclinic wave life-cycle behavior. *Quart. J. Roy. Meteor. Soc.,* **119,** 17–55.

Trenberth, K. E., and J. G. Olson, 1988: An evaluation and intercomparison of global analyses from the National Meteorological Center and the European Centre for Medium Range Weather Forecasts. *Bull. Amer. Meteor. Soc.,* **69,** 1047–1057.

Troup, A. J., and N. A. Streten, 1972: Satellite-observed Southern Hemisphere cloud vortices in relation to conventional observations. *J. Appl. Meteor.,* **11,** 909–917.

Uccellini, L. W., 1990: Processes contributing to the rapid development of extratropical cyclones. *Extratropical Cyclones. The Erik Palmén Memorial Volume,* C. W. Newton and E. O. Holopainen, Eds., Amer. Meteor. Soc., 81–105.

——, and P. J. Kocin, 1987: The interaction of jet streak circulations during heavy snow events along the east coast of the United States. *Wea. Forecasting,* **2,** 289–308.

——, ——, R. A. Petersen, C. H. Wash, and K. F. Brill, 1984: The Presidents' Day cyclone of 18–19 February 1979: Synoptic overview and analysis of the subtropical jet streak influencing the pre-cyclogenetic period. *Mon. Wea. Rev.,* **112,** 31–55.

Weldon, R. B., 1977: An oceanic cyclogenesis—Its cloud pattern interpretation. NWW/NESS Satellite Applications Information Note 77/7, 11 pp.

Young, M. V., 1993: Cyclogenesis: Interpretation of satellite and radar images for the forecaster. Forecasting Research Division Tech. Rep. 73. [Available from Forecasting Research Division, Meteorological Office, London Rd., Bracknell, Berkshire RG12 2SZ, United Kingdom.]

Zillman, J. W., and P. G. Price, 1972: On the thermal structure of mature Southern Ocean cyclones. *Aust. Meteor. Mag.,* **20,** 34–48.